

Upgrading a high-throughput spectrometer for high-frequency (

T. Nishizawa, M. D. Nornberg, D. J. Den Hartog, and D. Craig

Citation: *Review of Scientific Instruments* **87**, 11E530 (2016); doi: 10.1063/1.4960073

View online: <http://dx.doi.org/10.1063/1.4960073>

View Table of Contents: <http://scitation.aip.org/content/aip/journal/rsi/87/11?ver=pdfcov>

Published by the [AIP Publishing](#)

Articles you may be interested in

[Observation of 20–400 kHz fluctuations in the U-3M torsatron](#)

Phys. Plasmas **23**, 022506 (2016); 10.1063/1.4942419

[Development and validation of a 10 kHz–1 MHz magnetic susceptometer with constant excitation field](#)

J. Appl. Phys. **111**, 07E349 (2012); 10.1063/1.3680200

[Angular dependence of high-frequency seafloor acoustic backscatter \(200–400 kHz\)](#)

J. Acoust. Soc. Am. **130**, 2349 (2011); 10.1121/1.3654410

[A 2 kHz–100 MHz dynamic amplifier for tracking targets of variable amplitude](#)

Rev. Sci. Instrum. **72**, 2756 (2001); 10.1063/1.1374598

[Low-cost modification for the high-frequency raster on the Cameca IMS-3F secondary ion mass spectrometer](#)

J. Vac. Sci. Technol. A **17**, 317 (1999); 10.1116/1.581587



Upgrading a high-throughput spectrometer for high-frequency (<400 kHz) measurements

T. Nishizawa,^{1,a)} M. D. Nornberg,¹ D. J. Den Hartog,¹ and D. Craig²

¹University of Wisconsin–Madison, Madison, Wisconsin 53706, USA

²Wheaton College, Wheaton, Illinois 60187, USA

(Presented 8 June 2016; received 3 June 2016; accepted 8 July 2016;

published online 22 August 2016)

The upgraded spectrometer used for charge exchange recombination spectroscopy on the Madison Symmetric Torus resolves emission fluctuations up to 400 kHz. The transimpedance amplifier's cutoff frequency was increased based upon simulations comparing the change in the measured photon counts for time-dynamic signals. We modeled each signal-processing stage of the diagnostic and scanned the filtering frequency to quantify the uncertainty in the photon counting rate. This modeling showed that uncertainties can be calculated based on assuming each amplification stage is a Poisson process and by calibrating the photon counting rate with a DC light source to address additional variation. *Published by AIP Publishing.* [<http://dx.doi.org/10.1063/1.4960073>]

I. INTRODUCTION

The Ion-Doppler Spectrometer II (IDSII) used for Charge Exchange Recombination Spectroscopy (CHERS)¹ was originally designed to measure ion dynamics associated with tearing modes with frequencies up to 50 kHz. We could also address the physics of plasma fluctuations at higher frequencies, e.g., micro-instabilities^{2,3} and Alfvénic fluctuations associated with energetic particle modes,⁴ by increasing the bandwidth of the spectrometer electronics to 400 kHz. We developed a model that generates synthetic digitized signals to facilitate the uncertainty estimation in the spectroscopic measurements and the bandwidth optimization. We found that it was important to maintain photon counting accuracy while increasing the filter frequency to find the optimum bandwidth of the detectors.

II. PHOTON DETECTION MODELING

We modeled each stage of the photon detection process to investigate how the photon counting rate is affected by the cutoff-frequency of the transimpedance amplifier, f_{3dB} . We use photomultiplier tubes (PMTs) and transimpedance amplifiers to convert diffracted light from the spectrometer to voltage signals. The transimpedance amplifiers also shape the raw PMT signals to allow digitization at 1 MHz without aliasing. The generation of photoelectrons on a photo-cathode obeys Poisson statistics. We assumed that the number of electrons ejected by a single primary electron on a dynode also obeys Poisson statistics⁵ with a probability distribution

$$P_{\mu}(n) = \frac{\mu^n e^{-\mu}}{n!}, \quad (1)$$

where μ is the expectation value and n is the number of secondary electrons ejected by the primary electron. The electron multiplication governed by this statistical process repeats at each dynode inside the PMT.

Therefore, the probability distribution for the PMT gain, Q , is given by

$$Q(G) = \sum_{n_1=0}^{\infty} \sum_{n_2=0}^{\infty} \cdots \sum_{n_{l-1}=0}^{\infty} P_{\mu}(n_1) P_{n_1\mu}(n_2) \cdots P_{n_{l-1}\mu}(G), \quad (2)$$

where G is the PMT gain and $l = 11$ is the number of dynodes. We simulated an output pulse of the transimpedance amplifier for a single photoelectron entering the PMT using a circuit simulator, LTspice,⁶ and superimposed a number of pulses to represent the signals in the photon counting measurements, shown Fig. 1(a). The variation in pulse heights corresponding to a single photoelectron is determined based on the PMT gain distribution given by Eq. (2). We chose a five-pole Bessel filter for pulse shaping due to its desirable characteristics of frequency response and varied f_{3dB} in the circuit model to optimize the bandwidth. To account for the digitizer's frequency response, the output of the transimpedance amplifier was averaged over the transient response time. The digitizer's bandwidth was neglected because it was sufficiently high compared with the simulated range of f_{3dB} . We sampled discrete points at a sampling frequency from the averaged signal and treated them as the synthetic signal in the model. This process is shown in Fig. 1(b).

III. UNCERTAINTY ESTIMATION THROUGH THE INTRODUCTION OF THE EFFECTIVE PHOTON COUNTING RATE

The photoelectron generation on a photo-cathode of the PMT is a Poisson stochastic process whose uncertainty is governed by the Poisson distribution. Additional sources of variation in the photon detection electronics, such as the discrete nature of photo-electrons, the statistical nature of

Note: Contributed paper, published as part of the Proceedings of the 21st Topical Conference on High-Temperature Plasma Diagnostics, Madison, Wisconsin, USA, June 2016.

^{a)}nishizawa@wisc.edu

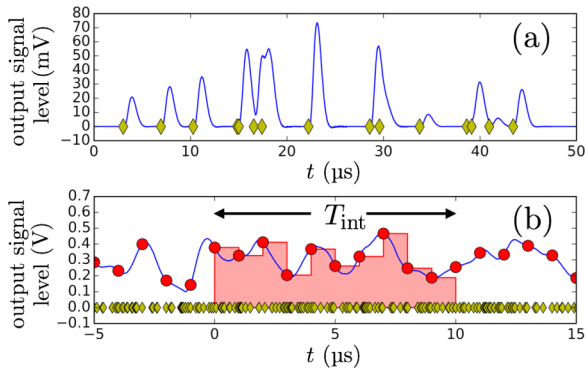


FIG. 1. (a) The blue line represents the transimpedance amplifier's output for a low photon counting rate. Each yellow diamond represents a photoelectron. (b) The blue line represents the averaged transimpedance amplifier's output over the transient response time of a digitizer. The red points represent digitized values. The red shaded area corresponds to a measurement of a number of photoelectrons over the integration time, $T_{\text{int}} = 10 \mu\text{s}$. The ratio of the area under the curve to the number of yellow diamonds (photoelectrons) fluctuates due to the processes described in the modeling indicating additional uncertainties.

photo-electron amplification, pulse shaping, and the finite sampling rate, add more variability in the measured signal. To estimate the total uncertainty in interpreting the photon counting rate from the measured output voltage of the transimpedance amplifier, we calculate an effective photon counting rate

$$\Phi_{\text{eff}} = \frac{\mu_V}{\sigma_V T_{\text{int}}}, \quad (3)$$

where μ_V is the mean signal level in voltage, σ_V is the standard deviation of the signal level, and T_{int} is the integration time. If there is a proportionality between the mean and the variance of the signals for photon count measurements, Φ_{eff} is proportional to the true photon counting rate.⁷ We measured Φ_{eff} by changing the mean signal level and plotted the results in Fig. 2(a). Figure 2(b) shows the relation between the true photon counting rate and Φ_{eff} for a synthetic signal using the model described in Section II where the true photon counting rate is given as a parameter for the simulation. A linear scaling can be seen for both plots in Fig. 2 indicating that $\Phi_{\text{eff}} T_{\text{int}}$ is proportional to the true photon counts and its standard deviation can be calculated from the mean value. The reduction in

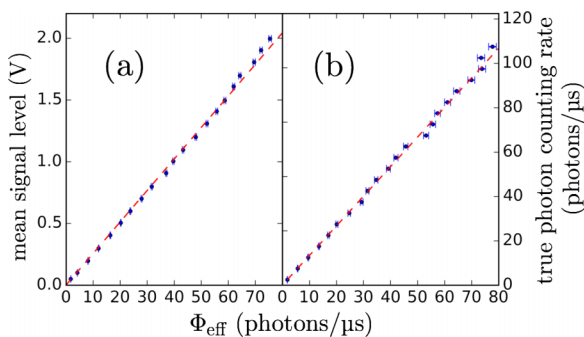


FIG. 2. (a) The effective photon counting rate measurement. An integrating sphere was used for a DC light source. (b) The simulation result for the relation between the photon counting rate and the effective photon counting rate. The simulation parameters, μ , and l were chosen to match the specifications of the PMT⁸ used in the measurements. $f_{3\text{dB}} = 400 \text{ kHz}$ for both (a) and (b).

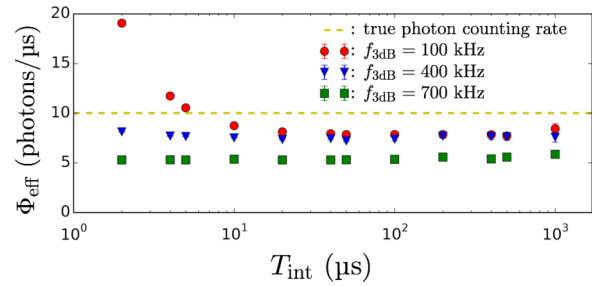


FIG. 3. Integration time vs effective photon counting rate for three different cutoff-frequencies. The true photon counting rate of $10 \text{ photons}/\mu\text{s}$ corresponds to a typical expected signal level.

Φ_{eff} from the photon counting rate seen in Fig. 2(b) is due to the increase in the fluctuation level of the signal caused by the sources of additional variability noted above.

We also investigated the dependence of Φ_{eff} on T_{int} for three different frequencies, $f_{3\text{dB}}$ using the synthetic signal model, shown in Fig. 3. The smoothing due to the low $f_{3\text{dB}}$ becomes dominant compared to the smoothing due to the integration in the case of short T_{int} resulting in effective photon counting rates higher than the true rate. High $f_{3\text{dB}}$ reduces the effective photon counting rate because of unattenuated spurious high frequency components resulting in larger signal variance.

IV. OPTIMIZING THE FILTER FOR TIME DYNAMIC SIGNALS

The brightness of an emission line from a plasma is not steady like the DC lamp, but changes over short time scales. While a low $f_{3\text{dB}}$ can increase Φ_{eff} when T_{int} is short, the instrument would not accurately resolve fluctuations of interest at high frequency. The optimization of the $f_{3\text{dB}}$ requires avoiding undercounting photons while preserving the high-frequency signal content. To find the optimum frequency, we ran simulations using synthetic signal modeling. This time, we turned off the statistical nature in the photo-electron

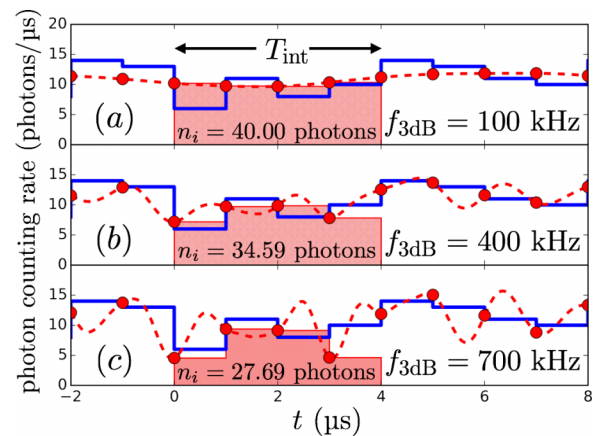


FIG. 4. Synthetic photon counts measurement for three different filter cutoff frequencies. $\Psi = 10 \text{ photons}/\mu\text{s}$, $T_{\text{int}} = 4 \mu\text{s}$ and $N_i = 35$ photons. The blue lines represent the true photon counting rate. The red points represent digitized values. The red shaded areas represents n_i for each cutoff-frequency. The area under the blue line between $0 \mu\text{s}$ and $4 \mu\text{s}$ corresponds to N_i .

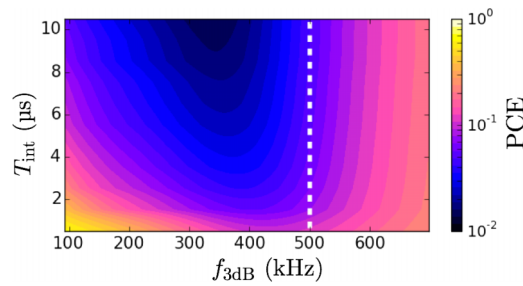


FIG. 5. Photon Counting Error (PCE) for the mean photon counting rate of 10 photons/ μ s. The white dashed line is the Nyquist frequency.

multiplication in the PMT and treated it as a constant to see the $f_{3\text{dB}}$ dependent part clearly. To compare the difference between the true and simulated photon counting rate, we evaluated the photon counting error (PCE),

$$\text{PCE} = \lim_{M \rightarrow \infty} \frac{1}{\Psi T_{\text{int}}} \sum_{i=1}^M \frac{(N_i - n_i)^2}{M}, \quad (4)$$

where M is the number of data points, Ψ is the mean photon counting rate, N_i is the true number of photon counts, and n_i is the measured photon counts. The time axis of the synthetic signal is shifted with respect to the true photon counting rate to correct for the phase delay introduced by the shaping amplifier. When the circuitry does not introduce any additional uncertainty, the PCE becomes 0. By contrast, when the signal averaging eliminates any observed time variability in signal, i.e., $n_i = \Psi T_{\text{int}}$, $\sum_{i=1}^M (N_i - n_i)^2 / M$ in Eq. (4) becomes a variance of a Poisson distribution. In this case, the PCE is unity since the mean and variance are the same. Three simulation examples for determining N_i and n_i are shown in Fig. 4.

We calculated the PCE as a function of $f_{3\text{dB}}$ and T_{int} in Fig. 5. The dependence of the PCE on the photon counting rate is found to be negligible in simulations indicating that the scaling of the PCE in Fig. 5 holds for any relevant photon counting rate. Figure 4(a) shows a case where $f_{3\text{dB}}$ is too low. The original change in the true photon counting rate is blurred due to over-smoothing resulting in the direction of the gradient of the PCE pointing to the lower left in the bottom left shown in Fig. 5. On the other hand, when $f_{3\text{dB}}$ is too high, the sampling rate of 1 MHz is not sufficient and we under-sample the data. This case is illustrated in Fig. 4(c) and accounts for the direction of the gradient of the PCE above the Nyquist frequency in Fig. 5. Based on Fig. 5, we designed the cutoff-frequency of the five-pole Bessel filter in the transimpedance amplifier to be 400 kHz. This cutoff-frequency leaves the frequency components around 100 kHz unattenuated and, therefore, should adequately resolve the fluctuations of interest. We took preliminary data with the up-

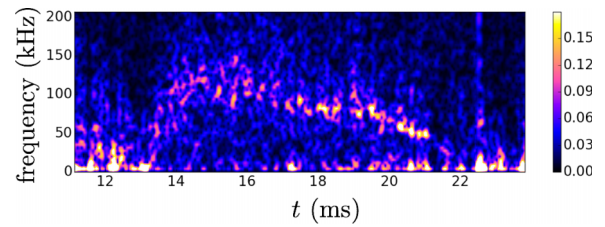


FIG. 6. Spectrogram for C III 229.7 nm electron impact emission observed in the edge of a 400 kA RFP plasma. The color represents the amplitudes with respect to the DC components.

graded amplifiers and successfully resolved frequencies near 100 kHz, shown Fig. 6.

V. SUMMARY

By modeling each stage of the spectrometer electronics chain we were able to optimize the bandwidth of the IDSII spectrometer to resolve emission fluctuations relevant for the study of microinstabilities and Alfvénic fluctuations due to fast particles. The optimization balances the need to keep the uncertainty level low while resolving fluctuations near 100 kHz. The upgraded spectrometer measurements successfully resolved fluctuations in the impurity emission line intensity near 100 kHz.

SUPPLEMENTARY MATERIAL

See [supplementary material](#) for the digital format of the data shown in this paper.

ACKNOWLEDGMENTS

This work is supported by the U.S. Department of Energy, Office of Science, and Office of Fusion Energy Sciences under Award No. DE-FC02-05ER54814.

¹D. Craig, D. J. Den Hartog, D. A. Ennis, S. Gangadhara, and D. Holly, *Rev. Sci. Instrum.* **78**, 013103 (2007).

²D. Carmody, M. J. Pueschel, and P. W. Terry, *Phys. Plasmas* **20**, 052110-1 (2013).

³D. Carmody, M. J. Pueschel, J. K. Anderson, and P. W. Terry, *Phys. Plasmas* **22**, 012504-1 (2015).

⁴L. Lin, J. K. Anderson, D. L. Brower, W. Capecchi, W. X. Ding, S. Eilerman, C. B. Forest, J. J. Kollner, D. Liu, M. D. Nornberg, J. Reusch, and J. S. Sarff, *Phys. Plasmas* **21**, 056104 (2014).

⁵Photomultiplier Tubes Basics and Applications, 3rd ed. (Edition 3a), Hamamatsu Photonics, (2007), p. 127.

⁶LTspice IV, <http://www.linear.com/designtools/software/>.

⁷Z. Liu, W. Hunt, M. Vaughan, C. Hostetler, M. McGill, K. Powell, D. Winker, and Y. Hu, "Estimating random errors due to shot noise in backscatter lidar observations," *Appl. Opt.* **45**, 4437-4447 (2006).

⁸ET Enterprises Electron Tubes, 9125B Series Data Sheet, <https://my.et-enterprises.com/pdf/9125B.pdf>.